Dalton Transactions

Accepted Manuscript

ROYAL SOCIETY OF CHEMISTRY

www.rsc.org/dalton

Cite this: DOI: 10.1039/c0xx00000x

www.rsc.org/xxxxxx

ARTICLE TYPE

Ruthenium, osmium and rhodium complexes of 1, 4-diaryl 1, 4-diazabutadiene: radical *versus* non-radical states

Sarat Chandra Patra,[a] Amit Saha Roy,[a] Vadivelu Manivannan,[b] Thomas Weyhermüller*[c] and Prasanta Ghosh*[a]

Received (in XXX, XXX) Xth XXXXXXXXX 20XX, Accepted Xth XXXXXXXXX 20XX
DOI: 10.1039/b000000x

Ruthenium, osmium and rhodium complexes of 1,4-di(3-nitrophenyl)-1,4-diazabutadiene (L^{DAB}) of types *trans*-$[Ru^{II}(L^{DAB})(PPh_3)_2Cl_2]$ (**1**), *trans*-$[Os^{II}(L^{DAB})(PPh_3)_2Br_2]$ (**2**) and *trans*-$[Rh(L^{DAB})(PPh_3)_2Cl_2]$ (**3**) are isolated and characterized by elemental analyses, IR, mass and ^{1}H NMR spectra including the single crystal X-ray structure determination of **1**.2toluene. The α-diimine fragment of the L^{DAB} ligand in **1**.2toluene is deformed showing a relatively longer -C=N- bond, 1.320 Å, and a shorter =CH-CH= bond, 1.395 Å. Density functional theory (DFT) calculations on *trans*-$[Ru(L^{DAB})(PMe_3)_2Cl_2]$ ($\mathbf{1}^{Me}$) and *trans*-$[Os(L^{DAB})(PMe_3)_2Br_2]$ ($\mathbf{2}^{Me}$) with singlet spin states authenticated that the closed shell singlet state (CSS) solutions of **1** and **2** are stable and no perturbation due to diradical open shell singlet (OSS) state is observed. The EPR spectra of **3** and the Mulliken spin density distribution obtained from the DFT calculation on *trans*-$[Rh(L^{DAB})(PMe_3)_2Cl_2]$ ($\mathbf{3}^{Me}$) infer that the ground electronic state of **3** can be defined by the $[Rh^{III}(L^{DAB\bullet-})(PPh_3)_2Cl_2]$ ($\mathbf{3}^{RhL\bullet}$) ↔ $[Rh^{II}(L^{DAB})(PPh_3)_2Cl_2]$ ($\mathbf{3}^{Rh\bullet L}$) resonating states. In solid, the contribution of $\mathbf{3}^{RhL\bullet}$ is higher and the g_{av} is 2.018 with Δg = 0.10, while in frozen glasses the contribution of $\mathbf{3}^{Rh\bullet L}$ is higher and the g_{av} is 2.026 with Δg (frozen glasses) = 0.13. The g parameters of the electrogenerated $[\mathbf{1}]^+$ (g_1 = 2.456, g_2 = 2.128 and g_3 = 1.624, Δg = 0.824), $[\mathbf{2}]^+$ (g_1 = 2.599, g_2 = 2.041 and g_3 = 1.965, Δg = 0.634), $[\mathbf{1}]^-$ (g_1 = 2.138, g_2 = 2.109, g_3 = 1.978 and Δg = 0.160) and $[\mathbf{2}]^-$ (g_1 = 2.168, g_2 = 2.097, g_3 = 1.987 and Δg= 0.181) ions and the spin density distributions obtained from the DFT calculations on $[\mathbf{1}^{Me}]^+$, $[\mathbf{2}^{Me}]^+$, $[\mathbf{1}^{Me}]^-$ and $[\mathbf{2}^{Me}]^-$ reveal that the reversible anodic peak of **1** and **2** at 0.11 and 0.34 V, referenced vs Fc^+/Fc couple are due to the M(III)/M(II) redox couple, while the reversible cathodic waves at -1.27 V and -0.82 V of **1** and **2** are due to L^{DAB}/ $L^{DAB\bullet-}$ redox couple. Both $[M^{II}(L^{DAB\bullet-})(PPh_3)_2Br_2]^-$ and $[M^{I}(L^{DAB})(PPh_3)_2Br_2]^-$ tautomers contribute to the ground electronic states of $[\mathbf{1}]^-$ (g = 2.075) and and $[\mathbf{2}]^-$ (g = 2.084) ions which are isoelectronic to **3**. Time dependent (TD) DFT calculations and spectroelectrochemical measurements elucidated that lower energy absorption bands of **1** and **2** are due to the metal to ligand charge transfer (MLCT) that disappears upon oxidation or reduction.

Introduction

Bistable electronic state of a molecule is the origin of the intramolecular electron transfer leading to the valence tautomerization (VT). Co-existence of the two redox centres creates a possibility to have a bistable electronic state in a molecule. In this context, coordination of a redox non-innocent organic molecule to the redox active transition metal ions opens up a path to generate a bistable electronic state in a molecule. Although, redox active organic ligands which are numerous now, VT reported so far is mostly limited to the transition metal complexes incorporating dioxolene type ligands.[1] Recently, an example of valence tautomerization with a copper (II) helicate of a non-dioxolene redox-active nitrogenous heterocyclic ligand has been reported.[2]

A coordinated α-diimine fragment (-N=CH-CH=N-) is isoelectronic to the α-diketone moiety (O=C(R)-C(R)=O) and is redox non-innocent[3-5] which exists in complexes in three redox states as neutral diimine (L^RR_2'), monoanionic diimine anion radical ($L^RR_2'^{\bullet-}$) and di-anionic diimide ($L^RR_2'^{2-}$) as illustrated in Scheme 1. Other way that distorts the coordinated diimine fragment is the 'back-bonding' of the filled metal d-orbitals with the unoccupied π* ($\pi^* = \pi_{diimine}^*$) orbital.[6]

Scheme 1

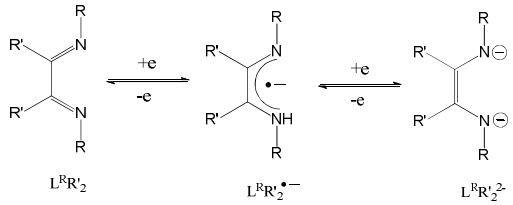

Thus, the elucidation of the electronic state of the L^RR_2' unit coordinated to a redox active metal ion (M^{n+}) is complex,

particularly when the reduction potentials ($E^0_{M(n+1)+/Mn+}$ and $E^0_{L/L^{\bullet-}}$) of the two redox reactions, $M^{(n+1)+} + e = M^{n+}$, and $L^RR_2' + e = L^RR_2'^{\bullet-}$, are comparable.

In such case, the $[M(L^RR_2')]^{n+}$ unit is expected to exhibit VT which is reported particularly with catechols/benzosemiquinone and (disalicylidene)diamine ligands coordinated to transition metal ions.[7] However, no valence tautomerization of a α-diimine transition metal complex as depicted in Scheme 2 has been substantiated so far.

Scheme 2

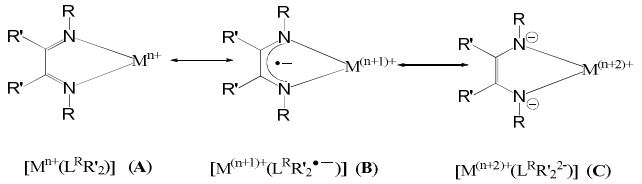

$[M^{n+}(L^RR'_2)]$ **(A)** $[M^{(n+1)+}(L^RR'^{\bullet-}_2)]$ **(B)** $[M^{(n+2)+}(L^RR'^{2-}_2)]$ **(C)**

In this work, we have successfully isolated the coordination complexes of L^{DAB} with ruthenium, osmium and rhodium ions using triphenyl phosphine and halides as co-ligands. New α-diimine complexes of types $[Ru^{II}(L^{DAB})(PPh_3)_2Cl_2]$ (**1**), $[Os^{II}(L^{DAB})(PPh_3)_2Br_2]$ (**2**) and $[Rh(L^{DAB})(PPh_3)_2Cl_2]$ (**3**) isolated in this work are depicted in Chart 1. A complete experimental and density functional theory (DFT) investigation has revealed that the ground electronic states of **1** and **2** are defined by the electronic state of type **A**, while **3** exists with a labile bistable electronic state having the contributions of types **A** and **B** of Scheme 2, which are abbreviated by $[Rh^{III}(L^{DAB\bullet-})(PPh_3)_2Cl_2]$ ($\mathbf{3}^{RhL\bullet}$) and $[Rh^{II}(L^{DAB})(PPh_3)_2Cl_2]$ ($\mathbf{3}^{Rh\bullet L}$) as illustrated in Chart 1. In this article, syntheses, spectra, molecular and electronic structures of **1**, **2** and **3**, including the electronic structures of $[\mathbf{1}]^+$, $[\mathbf{1}]^-$, $[\mathbf{2}]^+$ and $[\mathbf{2}]^-$ are reported.

Chart 1

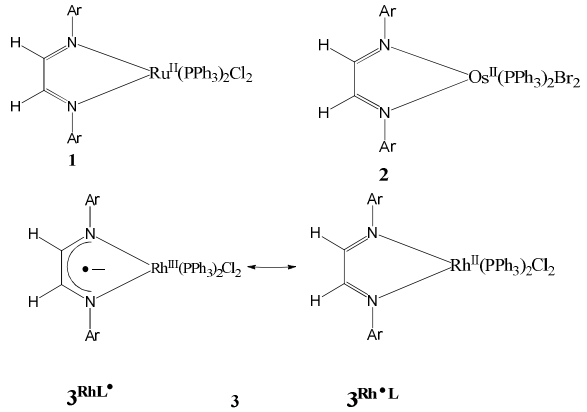

1 **2**

$\mathbf{3}^{RhL\bullet}$ **3** $\mathbf{3}^{Rh\bullet L}$

Experimental section

Physical measurements

Reagents and analytical grade materials were obtained from commercial suppliers and used without further purification. Spectroscopic grade solvents were used for spectroscopic and electrochemical measurements. The C, H and N content of the compounds were obtained from Perkin-Elmer 2400 series II elemental analyzer. Infrared spectra of the samples were measured from 4000 to 400 cm^{-1} as KBr pellets at room temperature on a Perkin-Elmer Spectrum RX1, FT-IR spectrophotometer. ^1H NMR spectrum in DMSO-d_6 and $CDCl_3$ solvents was carried out on a Bruker DPX-300 MHz spectrometer. ESI mass spectra ware recorded on a micro mass Q-TOF mass spectrometer. Electronic absorption spectra in solution at 298 K ware measured on a Perkin-Elmer Lambda 750 spectrophotometer in the range of 3300-175 nm. The X-band electron paramagnetic resonance (EPR) spectra at variable temperatures (298-110 K) were measured on a Magnettech GmbH MiniScope MS400 spectrometer (equipped with temperature controller TC H03), where the microwave frequency was measured with a frequency counter FC400. Magnetic susceptibility at 298 K was measured on Sherwood Magnetic Susceptibility Balance. The electro analytical instrument, BASi Epsilon-EC was used for cyclic voltammetric experiment and spectroelectrochemistry measurements. All the EPR spectra were simulated using Easy Spin software.

Syntheses

Glyoxalbis(3-nitrophenyl)imine (L^{DAB}). To a solution of 3-nitroaniline (1.38 g, 10 mmol) in methanol, glyoxal (0.29 g, 5 mmol) was added and the resulting mixture was stirred for 30 min at 25 °C. A yellow solid separated out, which was filtered and dried in air. Yield: 1.2 g (80%). ESI (positive ion)-MS in CH_3OH; *m/z* 299.03 for $[M]^+$. ^1H NMR (DMSO-d_6, 300 MHz): δ (ppm) = 7.47 (d, 2H, Ph), 7.40 (t, 2H, Ph), 7.25 (d, 2H, Ph), 6.91 (d, 2H, Ph), 4.94 (d, 2H, -N=CH-).Anal. Calcd for $C_{14}H_{10}N_4O_4$: C, 56.38; H, 3.38; N, 18.78. Found: C, 55.78; H, 3.23; N, 18.25. IR/cm^{-1} (KBr): ν = 3409 (s), 1619 (m), 1526 (vs), 1339 (vs), 1119 (m), 1051 (m), 901 (m), 861 (m), 734 (s), 670 (m).

***trans*-[Ru(L^{DAB})(PPh_3)$_2$$Cl_2$] (1).** To a hot solution of L^{DAB} (30 mg, 0.1 mmol) in 30ml dry toluene, $[Ru(PPh_3)_3Cl_2]$ (100 mg, 0.104 mmol) was added and the resulting mixture was heated to reflux for 25 min. A violet solution was obtained, which was kept at 298 K for slow evaporation. After 6-7 days single crystals of **1**.2toluene were obtained. Yield: 60 mg (~60% with respect to ruthenium). After evaporating the solvent of crystallization in high vacuum, the analytical data are collected. ESI (positive ion)-MS in CH_3OH; *m/z*: 927.38 for $[M-2Cl]^+$, 662.82 for [M-(PPh_3, 2Cl)]. ^1H NMR ($CDCl_3$, 300 MHz): δ (ppm) = 7.76 (s, 2H, Ph), 7.69 (d, 2H, Ph), 7.54 (d, 2H, Ph), 7.47 (d, 6H, Ph, PPh_3), 7.11 (t, 18H, Ph, PPh_3), 6.94 (d, 6H, PPh_3), 6.82 (s, 2H, =CH-CH=), 6.69 (t, 2H, Ph). Anal. Calcd for $C_{50}H_{40}Cl_2N_4O_4P_2Ru$: C, 60.37; H, 4.05; N, 5.63. Found: C, 60.07; H, 4.02; N, 5.48. IR/cm^{-1} (KBr): ν = 1585 (w), 1529 (vs), 1480 (m), 1457 (m), 1433 (s), 1349 (s), 1089 (s), 740 (s), 695 (vs), 541 (s), 522 (vs).

***trans*-[Os(L^{DAB})(PPh_3)$_2$$Br_2$] (2).** To a hot solution of L^{DAB} (30 mg, 0.1 mmol) in 30 ml dry toluene, $[Os(PPh_3)_3Br_2]$ (100 mg, 0.081 mmol) was added and the resulting mixture was heated to reflux under argon atmosphere for 1 hr. A brown colored solution was obtained. Dark brown crystalline compounds were obtained after slow evaporation of the solvent within 3-4 days). Yield: 40 mg (~40% with respect to osmium). ESI (positive ion)-MS in CH_3OH; *m/z*: 1090.21 for $[M-Br]^+$. ^1H NMR ($CDCl_3$, 300 MHz): δ (ppm) = 7.70 (s, 2H, Ph), 7.68 (d, 2H, Ph), 7.63 (s, 2H, =CH-CH=), 7.55 (t, 18H, Ph, PPh_3), 7.47 (d, 12H, Ph, PPh_3), 7.09 (t, 2H, Ph), 6.84 (d, 2H, Ph). Anal. Calcd for $C_{50}H_{40}Br_2N_4O_4P_2Os$: C, 51.20; H, 3.44; N, 4.78. Found: C, 49.88; H, 3.39; N, 4.69. IR/cm^{-1} (KBr): ν = 1618 (m), 1528 (vs), 1482 (m), 1434 (s), 1349

(vs), 1089 (m), 746 (m), 696 (vs), 518 (vs).

***trans*-[Rh($L^{DAB\bullet-}$)(PPh_3)$_2Cl_2$] (3).** To a hot solution of L^{DAB} ligand (150 mg, 0.5 mmol) in absolute dry ethanol (30 ml), $RhCl_3$ (100 mg, 0.5 mmol) and PPh_3 (300 mg, 1.2 mmol) were added successively and the reaction mixture was refluxed for 40 min (78 °C) under argon. A red solid separated out. The solution mixture was cooled at 20 °C and filtered. The residue was dried in air and collected. Yield: 150 mg (~ 30% with respect to rhodium). ESI (positive ion)-MS in $CHCl_3$; *m/z*: 999.15 for $[\mathbf{3}]^+$. Anal. Calcd for $C_{50}H_{42}Cl_2N_4O_4P_2Rh$: C, 60.13; H, 4.24; N, 5.61. Found: C, 59.83; H, 4.19; N, 5.50. IR/ cm^{-1} (KBr): ν = 1617 (m), 1528 (vs), 1482 (s), 1435 (vs), 1349 (vs), 1092 (s), 745 (m), 722 (m), 693 (vs), 531 (s).

X-Ray crystallographic data collection and refinement (CCDC 994910)

Single crystal of **1**.2toluene was picked up with a nylon loop and mounted on a Bruker Kappa-CCD diffractometer equipped with a Mo-target rotating anode X-ray source and a graphite monochromator (Mo-Kα, λ = 0.71073 Å). Final cell constants were obtained from least squares fits of all measured reflections. Structure was readily solved by Patterson method and subsequent difference Fourier techniques. The crystallographic data are listed in Table 1. ShelXS97[8a], ShelXL97[8b] and ShelXL2013-2[8c] were used for the structure solution and refinement. All non-hydrogen atoms were refined anisotropically. Hydrogen atoms were placed at the calculated positions and refined as riding atoms with isotropic displacement parameters.

Table 1 Crystallographic data for **1**.2toluene

	1.2toluene		
formula	$C_{64}H_{56}Cl_2N_4O_4P_2Ru$	calcd (g cm^{-3})	1.386
Fw	1179.04	reflnscollected	36330
crystcolour	violet	unique reflns	6814
crystsyst	Monoclinic	reflns [$I > 2\sigma(I)$]	4798
space group	*C*2/c	λ (Å) / μ (mm^{-1})	0.71073/0.481
a (Å)	27.7677(3)	F(000)	2432
b (Å)	13.6919(2)	R1[a] [$I > 2\sigma(I)$]/ GOF[b]	0.0323/0.928
c (Å)	16.3250(2)	R1[a] (all data)	0.0553
β (deg)	114.4320(10)	wR2[c] [$I > 2\sigma(I)$]	0.0627
V ($Å^3$)	5650.85(12)	no. of param./ restr.	421/ 277
Z	4	residual density ($eÅ^{-3}$)	0.373
T (K)	293(2)		

[a] $R1 = \Sigma||F_o|-|F_c||/\Sigma|F_o|$. [b] $GOF = \{\Sigma[w(F_o^2-F_c^2)^2]/(n-p)\}^{1/2}$. [c] $wR2 = [\Sigma[w(F_o^2-F_c^2)^2]/\Sigma[w(F_o^2)^2]]^{1/2}$ where $w = 1/[\sigma^2(F_o^2)+(aP)^2+bP]$, $P = (F_o^2+2F_c^2)/3$.

Density functional theory (DFT) calculations

All calculations reported in this article were done with the Gaussian 03W[9] program package supported by GaussView 4.1. The DFT[10] and TD DFT[11] calculations were performed at the level of Becke three parameter hybrid functional with the non-local correlation functional of Lee-Yang-Parr (B3LYP).[12] Gas-phase geometry of *trans*-[Ru(L^{DAB})(PMe_3)$_2Cl_2$] ($\mathbf{1}^{Me}$), *trans*-[Os(L^{DAB})(PMe_3)$_2Br_2$] ($\mathbf{2}^{Me}$) with singlet spin state were optimized using Pulay's Direct Inversion[13] in the Iterative Subspace (DIIS), 'tight' convergent SCF procedure[14] ignoring symmetry. Similarly, gas-phase geometry of *trans*-[Rh(L^{DAB})(PMe_3)$_2Cl_2$] ($\mathbf{3}^{Me}$), *trans*-[Ru(L^{DAB})(PMe_3)$_2Cl_2$]$^+$ $[\mathbf{1}^{Me}]^+$, *trans*-[Ru(L^{DAB})(PMe_3)$_2Cl_2$]$^-$ $[\mathbf{1}^{Me}]^-$, *trans*-[Os(L^{DAB})(PMe_3)$_2Br_2$]$^+$ $[\mathbf{2}^{Me}]^+$ and *trans*-[Os(L^{DAB})(PMe_3)$_2Br_2$]$^-$ $[\mathbf{2}^{Me}]^-$ were optimized using doublet spin state. In all calculations, a LANL2DZ basis set along with the corresponding effective core potential (ECP) was used for ruthenium, osmium and rhodium metals.[15] Valence double zeta basis set, 6-31G[16] for H was used. For C, O, P, Cl and Br non-hydrogen atoms valence double zeta with diffuse and polarization functions, 6-31+G*[17] as basis set was employed for all calculations. The percentage contributions of metal, chloride and bromide ligands to the frontier orbitals were calculated using GaussSum programme package.[18] The sixty lowest singlet excitation energies on each of the optimized geometries of $\mathbf{1}^{Me}$, $\mathbf{2}^{Me}$ and $\mathbf{3}^{Me}$ in CH_2Cl_2 using PCPM model were calculated by TD DFT method.[19] The natures of transitions were calculated by adding the probability of same type among alpha and beta molecular orbitals.

Results and discussions

Syntheses

Ruthenium, osmium and rhodium diimine complexes reported in this work are listed in Chart 1. **1** and **2** were synthesized from the reaction of $[M^{II}(PPh_3)_3X_2]$ precursors (M = Ru, X = Cl; M = Os, X = Br)[20] with L^{DAB}, while **3** was synthesized from a reaction of $RhCl_3$, PPh_3 and L^{DAB} ligand in boiling EtOH. All the complexes were characterized by elemental analyses, mass, IR and ^1H NMR spectra including the single crystal X-ray structure of **1**.2toluene. The UV-vis absorption spectra of **1**-**3** were recorded in CH_2Cl_2 at 298 K while the UV-vis absorption spectra of the corresponding $[\mathbf{1}]^+$, $[\mathbf{1}]^-$, $[\mathbf{2}]^+$, $[\mathbf{2}]^-$ ions were recorded by spectroelectrochemical measurements in CH_2Cl_2 (*vide infra*).

Molecular geometries

Molecular geometry of **1** in crystal was successfully confirmed by the single crystal X-ray structure of **1**.2toluene. **1**.2toluene crystallizes in *C*2/c space group. The molecular structure with the atom labelling scheme is depicted in Fig. 1 and the relevant bond parameters are summarized in Table 2. In **1**.2toluene, two PPh_3 ligands are trans to each other and the $RuP_2Cl_2N_2$ octahedron is distorted. The average Ru-P, Ru-Cl and Ru-N distances are 2.4179(5), 2.4206(5) and 2.0519(14) Å which correlate well with those reported in ruthenium (II) complexes of osazones of types **D** and **E** as shown in Chart 2.[6]

Chart 2

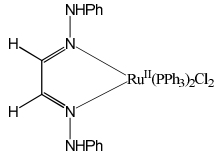

D

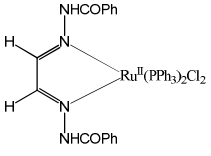

E

Bond parameters of the α-diimine fragment of the L^{DAB} ligand

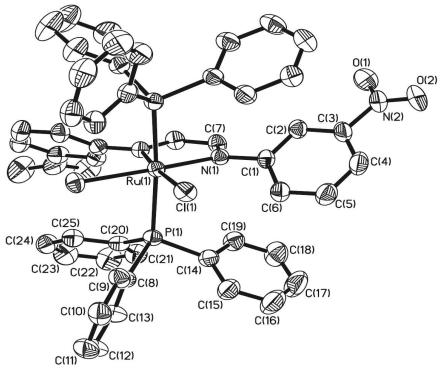

Fig. 1 Molecular geometry of **1**.2toluene in crystals (40% thermal ellipsoids; toluene molecule and H atoms are omitted for clarity).

are deviated from their ideal values. Two -N=C- lengths at 1.320 Å are longer, while the =CH-CH= length at 1.395(4) Å is shorter than expected. The features correlate well to those reported in the X-ray structures of **D** and **E** (Chart 2) which incorporate neutral diimine fragments coordinated to a ruthenium (II) ion. In this case also DFT calculations (*vide infra*) authenticated the existence of the neutral diimine fragment coordinated to ruthenium (II) ion in **1**.2toluene.

Table 2 Selected experimental and calculated bond lengths (Å) and angles (°) of **1**.2toluene

	Exp	Cal ($\mathbf{1}^{Me}$)		Exp	Cal ($\mathbf{1}^{Me}$)
Ru(1)-N(1)	2.0519 (14)	2.073	N(1)-Ru(1)-N(1A)	78.03(8)	78.06
Ru(1)-P(1)	2.4179 (5)	2.456	N(1)-C(7)-C(7A)	116.76 (10)	117.03
Ru(1)-Cl(1)	2.4206 (5)	2.477	C(7)-N(1)-Ru(1)	114.23 (12)	113.91
N(1)-C(7)	1.320(2)	1.328	Cl(1)-Ru(1)-N(1)	96.32(4)	95.38
C(7)-C(7A)	1.395(4)	1.409	P(1)-Ru(1)-P(1A)	170.37 (2)	163.02
N(1)-C(1)	1.437(2)	1.432			

EPR spectra

Magnetic susceptibility measurements at 298 K confirmed the paramagnetism of **3** (μ_{eff} = 1.89 μ_B). Variable temperature EPR spectra of **3** in solid, solution (~0.4 mM), and frozen glasses were recorded. The spectra are shown in Fig. 2 and Fig. 3 and the simulated EPR parameters are summarized in Table 3. It is encouraging that the EPR spectrum of the CH_2Cl_2 solution (at 293 K) of **3** at relatively lower concentration (~0.04 mM) displays hyperfine structures. The EPR spectrum is well simulated considering the hyperfine couplings due to diimine ^{14}N (A, 10.7 G) and ^{31}P (A, 21.4 G) nuclei as illustrated in Fig. S2, linewidth being only 1.2 G.

Chart 3

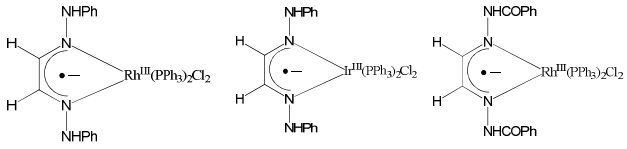

F **G** **H**

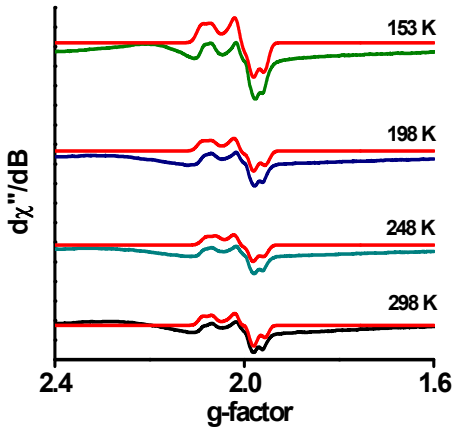

Fig. 2 Variable temperature EPR spectra of **3** in solid state (red = simulated spectra).

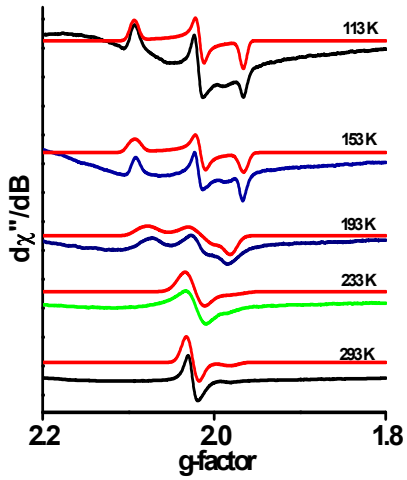

Fig. 3 Variable temperature EPR spectra of **3** in fluid solutions and frozen glasses of CH_2Cl_2 (red = simulated spectra).

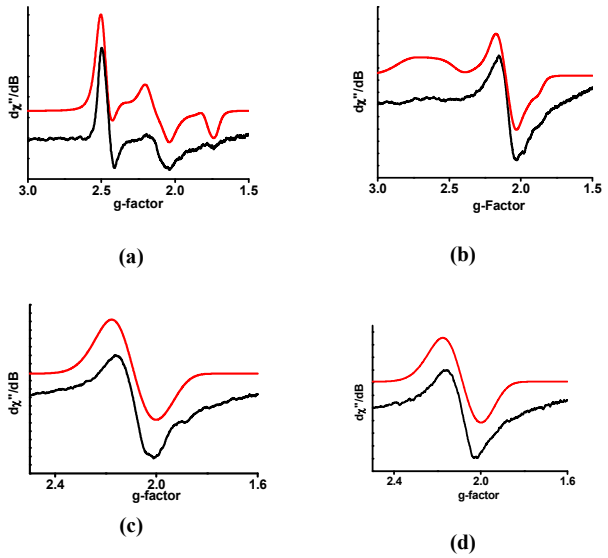

Fig. 4 EPR spectra of (a) $[\mathbf{1}]^+$, (b) $[\mathbf{2}]^+$, (c) $[\mathbf{1}]^-$ and (d) $[\mathbf{2}]^-$ in CH_2Cl_2-toluene frozen glasses at 110 K (black = experimental, red = simulated spectra).

Table 3 X-band EPR spectral parameters of **3**, $[\mathbf{1}]^+$, $[\mathbf{1}]^-$, $[\mathbf{2}]^+$ and $[\mathbf{2}]^-$

complexes	Conditions	Temp (K)	g_1	g_2	g_3	g_{av}	Δg	Linewidth (G); A (G)
3	Solid	298	2.079	1.999	1.975	2.018	0.10	2.7; ('^{103}Rh'; $A_1 = 32$, $A_2 = 32$, $A_3 = 40$)
		248	2.078	1.997	1.978	2.018	0.10	2.6; ('^{103}Rh'; $A_1 = 34$, $A_2 = 41$, $A_3 = 46$)
		198	2.076	1.991	1.986	2.018	0.09	2.5; ('^{103}Rh'; $A_1 = 34$, $A_2 = 43$, $A_3 = 50$)
		153	2.075	1.989	1.987	2.017	0.09	2.5; ('^{103}Rh'; $A_1 = 34$, $A_2 = 43$, $A_3 = 50$)
	CH_2Cl_2solution	293				2.025		2.5; ('^{14}N'; A = 6.3, '^{31}P' = 16.5)
	CH_2Cl_2solution	273				2.025		2.8; ('^{14}N'; A = 6.1, '^{31}P' = 16.1)
	CH_2Cl_2 solution	233				2.025		3.0 ('^{14}N'; A = 5.4, '^{31}P' = 12.9)
	CH_2Cl_2-frozen glass	193	2.082	2.017	1.980	2.026	0.102	2.5; ('^{103}Rh'; $A_1 = 25$, $A_2 = 27$, $A_3 = 14$)
	CH_2Cl_2-frozen glass	173	2.086	2.016	1.974	2.025	0.112	2.5
	CH_2Cl_2-frozen glass	153	2.094	2.017	1.966	2.026	0.128	1.5
	CH_2Cl_2-frozen glass	133	2.094	2.018	1.966	2.026	0.128	1.5
	CH_2Cl_2-frozen glass	113	2.094	2.017	1.966	2.026	0.128	1.5
$[\mathbf{1}]^+$	CH_2Cl_2-toluene frozen glass	110	2.456	2.128	1.624	2.069	0.824	4.0; ('^{101}Ru'; $A_1 = 3.57$, $A_2 = 43$, $A_3 = 32$)
$[\mathbf{1}]^-$			2.138	2.109	1.978	2.075	0.160	21.0; ('^{14}N'; $A_1 = 1.8$, $A_2 = 0.4$, $A_3 = 2.5$)
$[\mathbf{2}]^+$			2.599	2.041	1.965	2.202	0.634	11.0; ('^{189}Os'; $A_1 = 107$, $A_2 = 0$, $A_3 = 153$)
$[\mathbf{2}]^-$			2.168	2.097	1.987	2.084	0.181	22.0; ('^{14}N'; $A_1 = 1.3$, $A_2 = 0.5$, $A_3 = 1.5$)

The simulated g value at 1.995 is consistent with the existence of $\mathbf{3}^{RhL^\bullet}$ in fluid solution. At higher concentration, the spectrum at 293 K becomes broader (A_N, 6.3 G; A_P, 16.5 G) as shown in Fig. 3. At lower temperature, $\mathbf{3}^{Rh\bullet L}$ state dominates and anisotropicity increases. At the temperature range of 298 -153 K, the solid state displays anisotropic EPR spectra which are simulated by the hyperfine coupling of the ^{103}Rh nucleus. The g_{av} of **3** in solid state is 2.018 in a temperature range of 153-298 K, while the frozen glasses (113-153 K) exhibit rhombic spectra with g_{av} = 2.026 (Table 3). The g_{av} values 2.018-2.026 are comparatively lower indicating a contribution of $\mathbf{3}^{RhL^\bullet}$ to the ground electronic state of **3**. Similar features of the electronic state of the rhodium and iridium complexes of types **F**, **G** and **H** (Chart 3) incorporating osazone ligands have been reported recently.[6a, 21] In solution, a significant contribution of the non-radical tautomer (**II**) to the $[M^{III}(L^{NHAr}H_2^{\bullet-})(PPh_3)_2Cl_2$ (**I**) ↔ $[M^{II}(L^{NHAr}H_2)(PPh_3)_2Cl_2$ (**II**)] (M = Rh, Ir) resonating states was predicted, while in solids tautomer (**I**) incorporating an osazone anion radical dominates in **F**, **G** and **H**.

Analyses affirm that the unpaired electron is not solely localized either on the rhodium ion or the diimine fragment and the ground electronic state of **3** is discernable by $\mathbf{3}^{RhL^\bullet}$ ↔ $\mathbf{3}^{Rh\bullet L}$ resonating states. The g_{iso} of **3** in CH_2Cl_2 at 293 K is 1.995-2.026 (Table 3). The anisotropicity (Δg) increases in the frozen glasses and the maximum anisotropicity recorded is 0.13 at 113 K (Figure 3), which is much lower than the anisotropicity in a pure rhodium (II) complex.[22] The comparatively lower anisotropicity (0.10) in solid over a temperature range reveals that the contribution of $\mathbf{3}^{RhL^\bullet}$ is higher to the $\mathbf{3}^{RhL^\bullet}$ ↔ $\mathbf{3}^{Rh\bullet L}$ resonance structures in solids in comparison to that in solution.

The EPR spectra of the electrogenerated $[\mathbf{1}]^-$, $[\mathbf{2}]^-$, $[\mathbf{1}]^+$ and $[\mathbf{2}]^+$ ions were recorded in CH_2Cl_2 frozen glasses at 110 K and the spectra are illustrated in Fig. 4. Simulated g parameters are listed in Table 3. A significant contribution of metal ion was recorded to the EPR spectra (panel (c) and (d) of Fig. 4) of the electrogenerated $[\mathbf{1}]^-$ and $[\mathbf{2}]^-$ ions. The simulated g values are $[\mathbf{1}]^-$; $g_1 = 2.138$, $g_2 = 2.109$, $g_3 = 1.978$ and $[\mathbf{2}]^-$; $g_1 = 2.168$, $g_2 = 2.097$ and $g_3 = 1.987$ with anisotropicities (Δg) of 0.160 and 0.181 respectively. Thus, in $[\mathbf{1}]^-$ and $[\mathbf{2}]^-$ ions similar to **3** the electron is localized on the metal ion as well as on the diimine fragment. The ground electronic state of $[\mathbf{1}]^-$ and $[\mathbf{2}]^-$ ions are thus defined by the $[M^{II}(L^{DAB\bullet-})(PPh_3)_2Br_2]^-$ ↔ $[M^{I}(L^{DAB})(PPh_3)_2Br_2]^-$ resonance states (M = Ru, Os). $[\mathbf{1}]^+$ and $[\mathbf{2}]^+$ ions display rhombic spectra (panels (a) and (b) of Fig. 4). The simulated g values and the anisotropicities of $[\mathbf{1}]^+$ ($g_1 = 2.456$, $g_2 = 2.128$ and $g_3 = 1.624$, $\Delta g = 0.824$) and $[\mathbf{2}]^+$ ($g_1 = 2.599$, $g_2 = 2.041$ and $g_3 = 1.965$, $\Delta g = 0.634$) ions are consistent with the existence of ruthenium (III) and osmium (III) ions in the cations.[23] It authenticates that the oxidations of **1** and **2** are due to the oxidation of the metal ions affording $[M^{III}(L^{DAB})(PPh_3)_2Cl_2]^+$ complexes.

Electrochemical studies

The redox activities of **1**-**3** in CH_2Cl_2 were investigated by cyclic voltammetry at 298 K. The cyclic voltammograms are shown in Fig. 5. Redox potential data are referenced to ferrocenium/ferrocene, Fc^+/Fc, couple and are summarized in Table 4. The anodic waves of **1** and **2** (panels (a) and (b) of Fig. 5) at 0.11 V ($E_{1/2}^1$) and 0.34 V are reversible and are assigned to the M^{III}/M^{II} redox couple (M =Ru, Os) authenticated by EPR spectra of the electrogenerated $[\mathbf{1}]^+$ and $[\mathbf{2}]^+$ cations as stated above. Similarly, the cathodic waves of **1** and **2** respectively at -1.27 V and -0.82 V are reversible due to the $L^{DAB}/L^{DAB\bullet-}$ redox couple. Formation of anion radicals are confirmed by the EPR spectra of the electrogenerated $[\mathbf{1}]^-$ and $[\mathbf{2}]^-$ ions (Fig.4 and Table 3). Thus the electron transfer series of **1** and **2** are defined by the eqn 1.

$$[M^{III}(L^{DAB})(PPh_3)_2X_2]^+ \underset{-e}{\overset{+e}{\rightleftharpoons}} [M^{II}(L^{DAB})(PPh_3)_2X_2] \underset{-e}{\overset{+e}{\rightleftharpoons}} [M^{II}(L^{DAB\bullet-})(PPh_3)_2X_2]^- \quad (1)$$

Table 4 Redox potentials of **1**-**3** in CH_2Cl_2 (0.20 M $[N(n\text{-}Bu)_4]PF_6$) at 298 K (referenced to ferrocenium/ferrocene, Fc^+/Fc, couple)

Complexes	E_P^1/V	$E_{1/2}^2$/V (ΔE^a/mV)	$E_{1/2}^3$/V (ΔE^b/mV)	E_P^4/V
1		+0.11 (91)	-1.27 (80)	
2		+0.34 (100)	-0.82 (90)	
3	-0.01			-1.66

E_P^1= anodic peak potential; [a]anodicpeak-to-peak separation; [b]cathodicpeak-to-peak separation; E_P^4 = cathodic peak potential

Both the anodic and the cathodic redox peaks of **3** are irreversible as observed in osazone analogues.[6a, 21] The anodic peak potential of **3** at -0.01 V is comparable to those reported in the diimine anion radical complexes of transition metal ions.[24] In

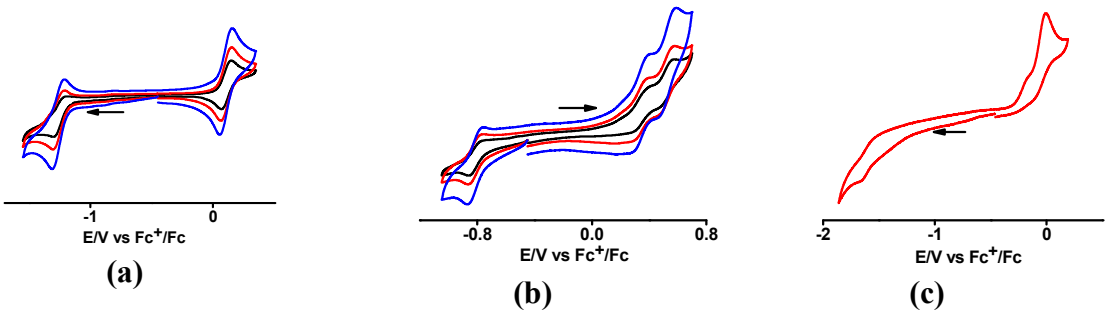

Fig. 5 Cyclic voltammograms of (a) **1** (scan rates: 50 (black), 100 (red), 200 (blue)), (b) **2** (scan rates: 50 (black), 100 (red), 200 (blue)), (c) **3** (scan rate: 50) in CH_2Cl_2 solvent at 298K. Conditions: 0.20 M $[N(n\text{-}Bu)_4]PF_6$ supporting electrolyte; platinum working electrode.

comparison to osazone analogues of rhodium and iridium (**F**, **G** and **H**) as shown in Chart 3, the anodic peak potential of **3** is at more negative. The anodic peak potentials of **F**, **G** and **H** are +0.13, +0.48 and +0.70 V.

Electronic structures

Ground state electronic structures of **1**-**3**, $[\mathbf{1}]^-$, $[\mathbf{2}]^-$, $[\mathbf{1}]^+$ and $[\mathbf{2}]^+$ were elucidated by the density functional theory (DFT) calculations. The gas phase geometries of *trans*-$[Ru(L^{DAB})(PMe_3)_2Cl_2]$ ($\mathbf{1}^{Me}$) and *trans*-$[Os(L^{DAB})(PMe_3)_2Br_2]$ ($\mathbf{2}^{Me}$) with singlet spin states and *trans*-$[Rh(L^{DAB})(PMe_3)_2Cl_2]$ ($\mathbf{3}^{Me}$), *trans*-$[Ru(L^{DAB})(PMe_3)_2Cl_2]^-$ $[\mathbf{1}^{Me}]^-$, *trans*-$[Os(L^{DAB})(PMe_3)_2Br_2]^-$ $[\mathbf{2}^{Me}]^-$, *trans*-$[Ru(L^{DAB})(PMe_3)_2Cl_2]^+$ $[\mathbf{1}^{Me}]^+$ and *trans*- $[Os(L^{DAB})(PMe_3)_2Br_2]^+$ $[\mathbf{2}^{Me}]^+$ with doublet spin states were optimized at the B3LYP level of the theory. The optimized geometries were illustrated in Fig. S1. The significant calculated bond parameters of $\mathbf{1}^{Me}$ are summarized in Table 2 and those of $\mathbf{2}^{Me}$, $\mathbf{3}^{Me}$, $[\mathbf{1}^{Me}]^-$, $[\mathbf{2}^{Me}]^-$, $[\mathbf{1}^{Me}]^+$ and $[\mathbf{2}^{Me}]^+$ are listed in Table 5.

The bond parameters of $\mathbf{1}^{Me}$ and $\mathbf{2}^{Me}$ listed in Tables 2 and 5 correlate well to those obtained from the single crystal X-ray structure determination of **1**.2toluene. It shows that the gross geometry of $\mathbf{1}^{Me}$ is very similar to that of **1** in crystals. In $\mathbf{1}^{Me}$, the calculated -C=N- and =CH-CH= lengths respectively are 1.328 and 1.409 Å, while calculated -C=N- and =CH-CH= lengths of $\mathbf{2}^{Me}$ are 1.342 and 1.396 Å. The calculated -C=N- and =CH-CH= lengths in the free $L^{Ph}H_2$ ligand are 1.280 and 1.474 Å.[25] The comparatively longer -C=N- and shorter =CH-CH= lengths are the features of the diimine anion radical authenticated by spectra and single crystal X-ray structure determinations.[4] As the diimine fragment is redox non-innocent, the ground electronic states of **1** and **2** are definable by the resonance structures of the closed

Chart 4

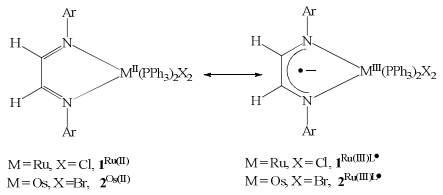

shell singlets ($\mathbf{1}^{Ru(II)}$ and $\mathbf{2}^{Os(II)}$) and the diradical open shell singlets ($\mathbf{1}^{Ru(III)L^{\bullet-}}$ and $\mathbf{2}^{Os(III)L^{\bullet-}}$) as depicted in Chart 4. However, the close shell singlet (CSS) solution of $\mathbf{1}^{Me}$ and $\mathbf{2}^{Me}$ are stable and no instabilities due to open shell singlet (OSS) perturbation have been established. Thus the possibility of the existence of OSS states, $\mathbf{1}^{Ru(III)L^{\bullet-}}$ and $\mathbf{2}^{Os(III)L^{\bullet-}}$ in **1** and **2** is discarded. Analyses of the molecular orbitals reveal a significant mixing of the d_{Ru} and d_{Os} with the π^* orbitals promoting electron transfer from the ruthenium (II) and osmium (II) ions to the ligand backbone. The calculated and experimental bond parameters qualitatively estimate the charge transfer from the ruthenium (II) and osmium (II) ions to the π^* orbital to the extent of 0.3-0.5e. The similar feature of the charge transfer from the ruthenium (II) and osmium (II) ions to the diimine fragment of osazone ligands is reported recently.[6] The ground electronic states of **1** and **2** are thus defined by the $\mathbf{1}^{Ru(II)}$ and $\mathbf{2}^{Os(II)}$ states (Chart 4) only.

The ground electronic state of **3** is different from those of **1** and **2**. The calculated –C=N- lengths are longer, while the –CH=CH- bond is comparatively shorter (Table 5). Mulliken spin density plot as depicted in panel (a) of Fig. 6 shows that, the unpaired electron of **3** is primarily localized on the diimine fragment. The calculated hyperfine coupling constants (A) due to ^{14}N and ^{31}P nuclei are 8.9 G and 19.5 G, while in solution, the A value decreases to 5.9 and 13.1 G respectively. The ground electronic state of **3** in gas phase corroborate to the $\mathbf{3}^{Rh(III)L^{\bullet-}}$ state as shown in Chart 1. However, the EPR spectra predicted a significant contribution of $\mathbf{3}^{Rh(II)L}$ state in solid, solution and glasses. Thus, the ground electronic state of **3** is defined by the $\mathbf{3}^{RhL^{\bullet}} \leftrightarrow \mathbf{3}^{Rh^{\bullet}L}$ resonating states.

Chart 5

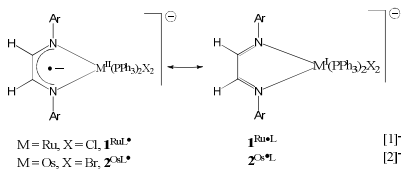

$[\mathbf{1}]^-$ and $[\mathbf{2}]^-$ ions are isoelectronic to **3**.The calculated significant bond parameters of $[\mathbf{1}^{Me}]^-$ and $[\mathbf{2}^{Me}]^-$ are comparable to those of $\mathbf{3}^{Me}$ (Table 5). The Mulliken spin densities are delocalized over both the metal and π^* orbitals as depicted in Fig. 6. The EPR spectra (panels (c) and (d) of Fig.4) also corroborate to the contribution of $[M^I(L^{DAB})(PPh_3)_2Br_2]^-$ state to $[\mathbf{1}]^-$ and $[\mathbf{2}]^-$

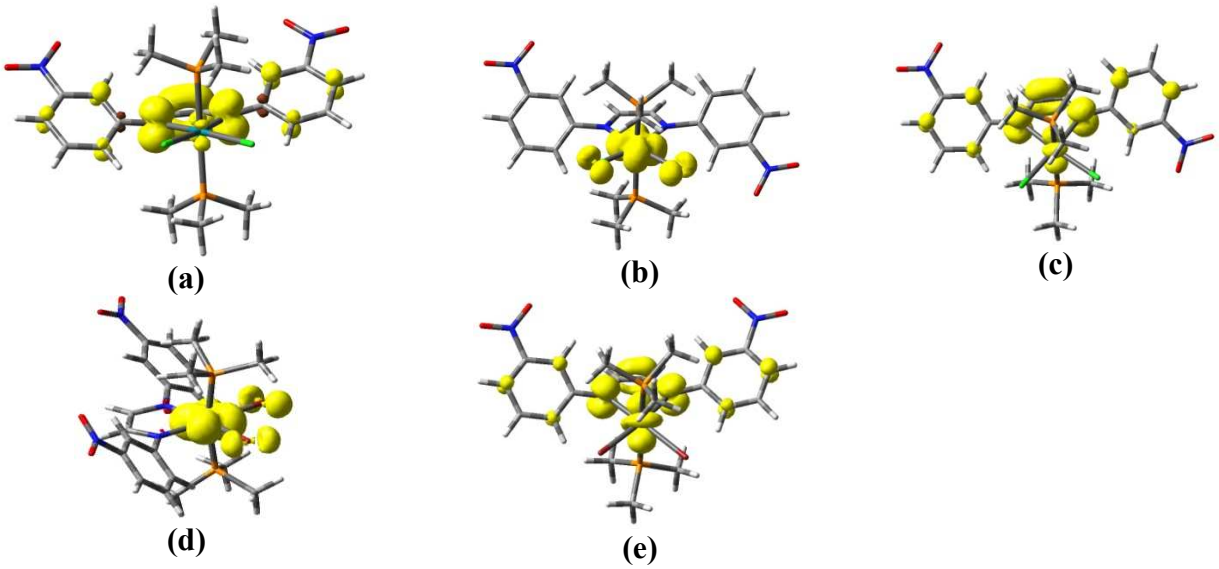

Fig. 6 Spin density plots of (a) $\mathbf{3}^{Me}$, (b) $[\mathbf{1}^{Me}]^+$, (c) $[\mathbf{1}^{Me}]^-$, (d) $[\mathbf{2}^{Me}]^+$ and (e) $[\mathbf{2}^{Me}]^-$ (isovalue = 0.004) and values from Mulliken spin population analyses (spin density, $\mathbf{3}^{Me}$: N1, 0.32, N4, 0.31, C2, 0.11, C3, 0.10, Rh, 0.01; $[\mathbf{1}^{Me}]^+$, Ru, 0.91, Cl1, 10, Cl2, 10; $[\mathbf{1}^{Me}]^-$, N1, 0.22, N4, 0.21, C2, 0.10, C3, 0.13, Ru, 0.17; $[\mathbf{2}^{Me}]^+$, Os, 0.90, Br1, 0.09, Br2, 0.09; $[\mathbf{2}^{Me}]^-$, N1, 0.17, N4, 0.19, C2, 0.10, C3, 0.06, Os, 0.22). Numbering scheme is shown in the illustration of Table 5.

Table 5 Selected calculated bond lengths (Å) of $\mathbf{2}^{Me}$, $\mathbf{3}^{Me}$, $[\mathbf{1}^{Me}]^-$, $[\mathbf{2}^{Me}]^-$, $[\mathbf{1}^{Me}]^+$ and $[\mathbf{2}^{Me}]^+$

	$\mathbf{2}^{Me}$	$\mathbf{3}^{Me}$	$[\mathbf{1}^{Me}]^-$	$[\mathbf{2}^{Me}]^-$	$[\mathbf{1}^{Me}]^+$	$[\mathbf{2}^{Me}]^+$
M-P	2.444	2.450	2.396	2.392	2.470	2.486
	2.431	2.424	2.398	2.388	2.509	2.477
M-X	2.649	2.490	2.541	2.691	2.360	2.528
	2.646	2.458	2.517	2.697	2.359	2.525
M-N1	2.059	2.107	2.164	2.114	2.143	2.099
M-N4	2.047	2.089	2.145	2.144	2.160	2.119
N1-C2	1.342	1.363	1.354	1.364	1.309	1.321
N4-C3	1.342	1.360	1.354	1.368	1.310	1.322
C2-C3	1.396	1.381	1.383	1.372	1.429	1.412

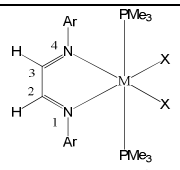

Ar = *m*-NO_2Ph,
M = Ru, X= Cl, $\mathbf{1}^{Me}$, $[\mathbf{1}^{Me}]^+$
M = Os, X= Br, $\mathbf{2}^{Me}$, $[\mathbf{2}^{Me}]^+$

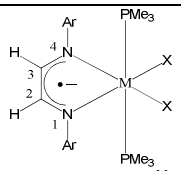

M = Ru, X= Cl, $[\mathbf{1}^{Me}]^-$
M = Os, X= Br, $[\mathbf{2}^{Me}]^-$
M = Rh, X= Cl, $\mathbf{3}^{Me}$

ions. Thus, the ground electronic states of $[\mathbf{1}]^-$ and $[\mathbf{2}]^-$ ions are surprisingly similar to that of **3** and described by the $[M^{II}(L^{DAB\bullet-})(PPh_3)_2Br_2]^- \leftrightarrow [M^{I}(L^{DAB})(PPh_3)_2Br_2]^-$ (M = Ru, Os) equilibrium as illustrated in Chart 5.

On the contrary to **1**-**3**, $[\mathbf{1}]^-$ and $[\mathbf{2}]^-$ ions, the calculated -C=N- lengths, 1.309 and 1.321 Å respectively of $[\mathbf{1}^{Me}]^+$ and $[\mathbf{2}^{Me}]^+$ ions are comparatively shorter, while the =CH-CH= bonds, 1.429 and 1.412 Å are longer. The trend of these bond lengths is consistent with the existence of neutral diimine fragments in $[\mathbf{1}]^+$ and $[\mathbf{2}]^+$ ions. The Mulliken spin densities are localized on the metal ions as shown in Fig. 6. In addition, the EPR spectra correlating the existence of ruthenium (III) and osmium (III) ions affirm that $[\mathbf{1}]^+$ and $[\mathbf{2}]^+$ ions are respectively the ruthenium (III) and osmium (III) complexes of L^{DAB} ligand as depicted in Chart 6.

Chart 6

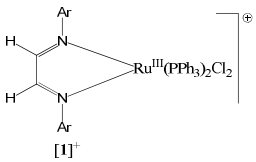

$[\mathbf{1}]^+$

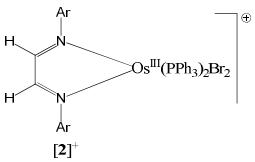

$[\mathbf{2}]^+$

Electronic spectra

UV-vis absorption spectra of the L^{DAB} ligand and the complexes were recorded in CH_2Cl_2 solvent at 298 K. Spectral data are listed in Table 6. The selected spectra are shown in Fig. 7. The solid state absorption spectrum (Kubelka–Munk plot)[26] of **3** was also

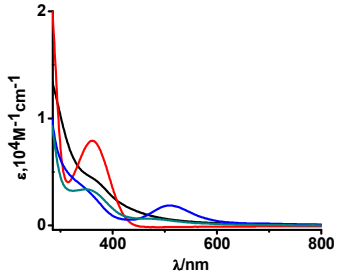

Fig. 7 Electronic absorption spectra of ligand (red), **1** (blue), **2** (green) and **3** (black) in CH_2Cl_2 at 298 K.

Table 6 UV-vis absorption spectral data of ligand and **1-3** in CH_2Cl_2 at 298 K

Substrates	λ_{max} (nm) (ε,10^4 M^{-1} cm^{-1})
L^{DAB}	360 (0.79)
1	509(0.19), 338 (0.38)
2	487 (0.06), 355 (0.33)
3	360 (0.44)

Table 7 Calculated and experimental excitation energies (λ/nm), oscillator strengths (f) and significant transitions of $\mathbf{1}^{Me}$, $\mathbf{2}^{Me}$ and $\mathbf{3}^{Me}$

λ_{calc} /nm	f	λ_{exp} /nm	significant contributions (>10%)	transition types	dominant contributions
			$\mathbf{1}^{Me}$		
499.05	0.0564	509	HOMO-2 → LUMO (61%)	$[d_{Ru} + p_{Cl}]$ (85%) + π_L (15%) → π^*_L (90%) + $[d_{Ru} + p_{Cl}]$ (10%)	MLCT
465.89	0.0482		HOMO-3 → LUMO (47%)	$[d_{Ru} + p_{Cl}]$ (70%) + π_L (30%)→ π^*_L (90%) + $[d_{Ru} + p_{Cl}]$ (10%)	MLCT
370.25	0.3676	338	HOMO-5 → LUMO (35%)	$[d_{Ru} + p_{Cl}]$ (75%) + π_L (25%)→ π^*_L (90%) + $[d_{Ru} + p_{Cl}]$ (10%)	MLCT
			$\mathbf{2}^{Me}$		
487.08	0.0313	487	HOMO-2→ LUMO (90%)	$[d_{Os} + p_{Br}]$ (70%) + π_L (30%) → π^*_L (87%) + d_{Os} (13%)	MLCT
366.98	0.1270	355	HOMO-5→ LUMO (42%)	$[d_{Os} + p_{Br}]$ (80%) + π_L (15%) → π^*_L (87%) + d_{Os} (13%)	MLCT
350.85	0.1357		HOMO-6→ LUMO (35%)	$[d_{Os} + p_{Br}]$ (84%) + $\pi_{Ph(L)}$ (16%) → π^*_L (87%) + d_{Os} (13%)	MLCT
			$\mathbf{3}^{Me}$		
503.72	0.1416	483	β-HOMO → β-LUMO (92%)	π_L (75%) + $[d_{Rh} + p_{Cl}]$ (25%) → π^*_L (98%) + $[d_{Rh} + p_{Cl}]$ (2%)	$\pi \rightarrow \pi^*$
390.98	0.1652		α-HOMO → α-LUMO + 4 (56%)	$\pi^*_{diimine}$ (98%) + $[d_{Rh} + p_{Cl}]$ (2%) → π^*_L (99%)	LLCT
369.37	0.0624	360	α-HOMO → α-LUMO + 4 (11%)	$\pi^*_{diimine}$ (98%) + $[d_{Rh} + p_{Cl}]$ (2%) → π^*_L (99%)	LLCT

recorded by the diffuse reflection method (Fig. 8). The free L^{DAB} ligand in CH_2Cl_2 absorbs strongly at 360 nm. **1** and **2** exhibit lower energy absorption bands at 509 and 487 nm, while **3** absorbs weakly at 480 nm, displaying no significant lower energy absorption band in the range of 800-2600 nm. It is significant to observe that in solid state, the absorption maximum of **3** is red shifted to 432 nm.

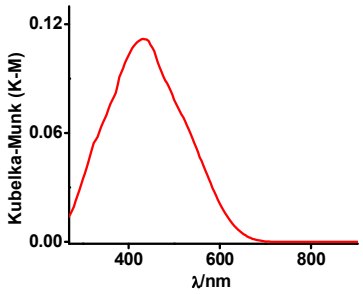

Fig. 8 Solid state UV-vis absorption spectrum of **3**.

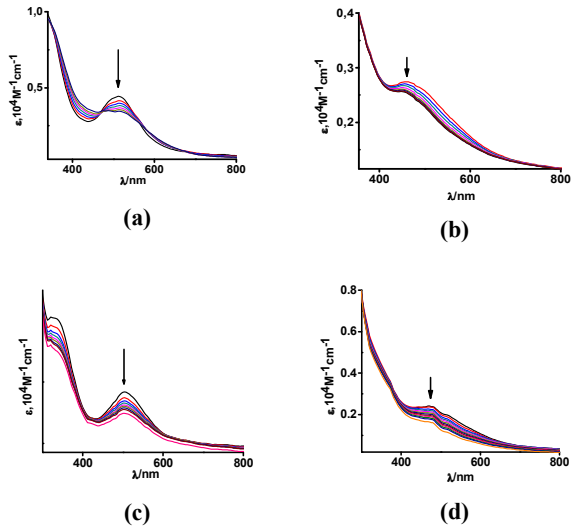

Fig. 9 Spectroelectrochemical measurements of **1** and **2** showing the change in electronic spectra of electrochemically generated (a) $[\mathbf{1}]^+$, (b) $[\mathbf{2}]^+$, (c) $[\mathbf{1}]^-$ and (d) $[\mathbf{2}]^-$ ions in CH_2Cl_2 at 298 K.

The origins of absorptions were elucidated by time dependent (TD) DFT calculations on $\mathbf{1}^{Me}$, $\mathbf{2}^{Me}$ and $\mathbf{3}^{Me}$ in CH_2Cl_2 using PCPM model. Excitation energies, oscillator strengths (f) and the transition types are listed in Table 7. The L^{DAB} ligand absorbs at 360 nm due to $\pi \rightarrow \pi^*$ transition. The lower energy absorption bands of **1** and **2** are due to metal to ligand charge transfer (MLCT). The weaker absorption band at 360 nm is due to the $\pi \rightarrow \pi^*$ (SOMO) transitions. The intensity of the MLCT bands of **1** and **2** gradually decreases during conversion of **1** → $[\mathbf{1}]^+$ and **2** → $[\mathbf{2}]^+$ ions as recorded by spectroelectrochemical measurements, which are illustrated in the panels (a) and (b) of Fig. 9. The feature is consistent with the oxidations of M (II) to M (III) ions. Similarly, the intensity of the MLCT transition decreases upon reductions of **1** → $[\mathbf{1}]^-$ and **2** → $[\mathbf{2}]^-$ ions as depicted in the panels (c) and (d) of Fig. 9. It is due to the conversion of $\pi \rightarrow \pi^*$ (SOMO).

Conclusions

A new family of α-diimine complexes of ruthenium, osmium and rhodium ions of type $[M(L^{DAB})PPh_3X_2]$ (M = Ru, X = Cl, **1**; M = Os, X = Br, **2**; M = Rh, X = Cl, **3**) was isolated and characterized by experimental and theoretical studies. Single crystal X-ray bond parameters of **1** and density functional theory (DFT) calculations on $\mathbf{1}^{Me}$ and $\mathbf{2}^{Me}$ established that the neutral diimine ligand (L^{DAB}) coordinates to ruthenium (II) and osmium (II) ions in **1** and **2**. The deformation of the coordinated diimine fragment in **1** and **2** is due to the strong $d_\pi \rightarrow d_{\pi^*}$ back-bonding. On the contrary, the solid and solution EPR spectra of **3** and the DFT calculation on $\mathbf{3}^{Me}$ elucidated the contribution of α-diimine anion radical ($\mathbf{3}^{RhL^\bullet}$) coordinated to the rhodium (III) ion in **3**.

The ground electronic state of **3** is thus defined by the $[Rh^{III}(L^{DAB\bullet-})(PPh_3)_2Cl_2]$ ($\mathbf{3}^{RhL^\bullet}$) ↔ $[Rh^{II}(L^{DAB})(PPh_3)_2Cl_2]$ ($\mathbf{3}^{Rh\bullet L}$) resonating states. In solution and frozen glasses, the contribution of the rhodium (II) tautomer ($\mathbf{3}^{Rh\bullet L}$) is relatively higher. **1** and **2** exhibit reversible anodic peaks at 0.11 and 0.34 V and reversible cathodic peaks at -1.27 and -0.82 V. The contributions of both $[M^{II}(L^{DAB\bullet-})(PPh_3)_2Br_2]^-$ and $[M^{I}(L^{DAB})(PPh_3)_2Br_2]^-$ (M = Ru, Os) tautomers to the ground electronic states of $[\mathbf{1}]^-$ and $[\mathbf{2}]^-$ ions which are isoelectronic to **3**, are predicted by the EPR spectra and DFT calculations, while the $[\mathbf{1}]^+$ and $[\mathbf{2}]^+$ ions are the pure ruthenium (III) and osmium (III) complexes of neutral diimine ligand (L^{DAB}). The lower energy absorption bands of **1** and **2**

respectively at 509 and 487 nm which are absent in free ligand, are due to the metal to ligand charge transfer (MLCT) elucidated by the TD DFT calculations on $\mathbf{1}^{Me}$ and $\mathbf{2}^{Me}$. The lower energy absorption bands of **1** and **2** disappear in $[\mathbf{1}]^+$, $[\mathbf{2}]^+$, $[\mathbf{1}]^-$ and $[\mathbf{2}]^-$ ions recorded by spectroelectrochemical measurements.

Acknowledgements

Financial support received from DST (SR/S1/IC/0026/2012) and CSIR 01(2699/12/EMR-II) New Delhi, India is gratefully acknowledged. SP is thankful to CSIR (CSIR No.: 08/531(0008)/2013 EMR-I), New Delhi, India for fellowship. PG is thankful to Alexander-von-Humboldt Foundation for fellowship.

Notes and references

[a]*Department of Chemistry, R. K. Mission Residential College, Narendrapur, Kolkata-700103, India.*
Fax: 91 33 2477 3597; Tel: 91 33 2428 7347; E-mail: ghosh@pghosh.in
[b]*Department of Chemistry, IIT Guwahati, Guwahati - 781 039, India*
[c]*Max-Planck Institute for Chemical Energy Conversion, Strifstr. 34-36, 45470 Muelheiman der Ruhr, Germany*

† Electronic Supplementary Information (ESI) available: X-ray crystallographic CIF file for the **1**.2toluene (CCDC 994910). Gas phase optimized geometries of $\mathbf{1}^{Me}$, $\mathbf{2}^{Me}$, $\mathbf{3}^{Me}$, $[\mathbf{1}^{Me}]^+$, $[\mathbf{2}^{Me}]^+$, $[\mathbf{1}^{Me}]^-$ and $[\mathbf{2}^{Me}]^-$, EPR measurement parameters, Experimental and simulated EPR spectra of **3** in CH_2Cl_2 solution at 273 K, CH_2Cl_2- frozen glasses at 273 and 133 K, Coordinates of the optimized geometries of $\mathbf{1}^{Me}$, $\mathbf{2}^{Me}$, $\mathbf{3}^{Me}$, $[\mathbf{1}^{Me}]^+$, $[\mathbf{2}^{Me}]^+$, $[\mathbf{1}^{Me}]^-$ and $[\mathbf{2}^{Me}]^-$. These materials are available free of charge *via* the internet.See DOI: 10.1039/b000000x/

1 (a) B. Li, L.-Q. Chen, R.-J. Wei, J. Tao, R-B. Huang, L-S. Zheng and Z. Zheng, *Inorg. Chem.,* 2011, **50**, 424; (b) G. Poneti, M. Mannini, L. Sorace, P. Sainctavit, M-A. Arrio, E. Otero, J. C. Cezar and A. Dei, *Angew. Chem., Int. Ed.,* 2010, **49**, 1954; (c) I. Imaz, D. Maspoch, C. Rodríguez-Blanco, J. M. Pérez-Falcón, J. Campo and D. Ruiz-Molina, *Angew. Chem., Int. Ed.,* 2008, **47**, 1857; (d) D. G. Lonnon, S. T. Lee and S. B. Colbran, *J. Am. Chem. Soc.,* 2007, **129**, 5800; (e) N. Shaikh, S. Goswami, A. Panja, X-Y. Wang, S. Gao, R. J. Butcher and P. Banerjee, *Inorg. Chem.,* 2004, **43**, 5908; (f) C. G. Pierpont, *Coord. Chem. Rev.,* 2001, **216-217**, 99; (g) C. G. Pierpont, *Coord. Chem. Rev.,* 2001, **219-221**, 415; (h) S. H. Bodner, A. Caneschi, A. Dei, D. A. Shultz and L. Sorace, *Chem. Commun*., 2001, 2150; (i) J. Rall, M. Wanner, M. Albrecht, F. M. Hornung and W. Kaim, *Chem.—Eur. J.,* 1999, **5**, 28026; (j) G. A. Abakumov, V. K. Cherkasov, V. I. Nevodchikov, V. A. Kuropatov, B. C. Noll and C. G. Pierpont, *Inorg. Chem.,* 1998, **37**, 6117; (k) A. S. Attia and C. G. Pierpont, *Inorg. Chem.,* 1998, **37**, 3051; (l) C. Roux, D. M. Adams, J. P. Itié, A. Polian, D. N. Hendrickson and M.Verdaguer, *Inorg. Chem.,* 1996, **35**, 2846; (m) O. S. Jung and C. G. Pierpont, *J. Am. Chem. Soc.,* 1994, **116**, 2229; (n) C. G. Pierpont and R. M. Buchanan, *Coord. Chem. Rev.,* 1981, **38**, 45.

2 N. Kundu, M. Maity, P. B. Chatterjee, S. J. Teat, A. Endo and M. Chaudhury, *J. Am. Chem. Soc.,* 2011, **133**, 20104.

3 (a) I. R. Corn, P. D. A. Sánchez, M. J. Zdilla, P. E. Fanwick, M. J. Shaw, J. T. Miller, D. H. Evans and M. M. Abu-Omar, *Inorg. Chem.,* 2013, **52**, 5457; (b) S. J. Kraft, U. J. Williams, S. R. Daly, E. J. Schelter, S. A. Kozimor, K. S. Boland, J. M. Kikkawa, W. P. Forrest, C. N. Christensen, D. E. Schwarz, P. E. Fanwick, D. L. Clark, S. D. Conradson and S. C. Bart, *Inorg. Chem*., 2011, **50**, 9838; (c) F. Hartl, M. P. Aarnts, H. A. Nieuwenhuis and J. V. Slageren, *Coord. Chem. Rev*., 2002, **230**, 107.

4 (a) V. Lorenz, C. G. Hrib, D. Grote, L. Hilfert, M. Krasnopolski and F. T. Edelmann, *Organometallics,* 2013, **32**, 4636; (b) W. Zhou, L. Chiang, B. O. Patrick, T. Storr and K. M. Smith, *Dalton Trans.,* 2012, **41**, 7920; (c) D. W. Shaffer, S. A. Ryken, R. A. Zarkesh and A. F. Heyduk, *Inorg. Chem.,* 2011, **50**, 13; (d) H. Tsurugi, T. Saito, H. Tanahashi, J. Arnold and K. Mashima, *J. Am. Chem. Soc.,* 2011, **133**, 18673; (e) M. M. Khusniyarov, T. Weyhermüller, E. Bill and K. Wieghardt, *J. Am. Chem. Soc.,* 2009, **131**, 1208 and relevant references therein; (f) E. Gore-Randall, M. Irwin, M. S. Denning and J. M.Goicoechea, *Inorg. Chem.,* 2009, **48**, 8304; (g) G. H. Spikes, S. Sproules, E. Bill, T. Weyhermüller and K. Wieghardt, *Inorg. Chem*., 2008, **47**, 10935 and refrences therein; (h) P. J. Bailey, C. M. Dick, S. Fabre, S. Parsons and L. J. Yellowlees, *Dalton Trans*., 2006, 1602; (i) H. M. Tuononen and A. F. Armstrong, *Dalton Trans.,* 2006, 1885; (j) H. M.Tuononen and A. F. Armstrong, *Inorg. Chem.,* 2005, **44**, 8277; (k) R. J. Baker, R. D. Farley, C. Jones, D. P. Mills, M. Kloth and D. M. Murphy, *Chem. Eur. J.,* 2005, **11**, 2972; (l) P. Ghosh, E. Bill, T. Weyhermuller, F. Neese and K. Wieghardt, *J. Am. Chem. Soc.,* 2003, **125**, 1293; (m) T. Pott, P. Jutzi, W. Kaim, W. W. Schoeller, B. Neumann, A. Stammler, H. G. Stammler, M. Wanner, *Organometallics,* 2002, **21**, 3169; (n) M. G. Gardiner, G. R. Hanson, M. J. Henderson, F. C. Lee and C. L. Raston, *Inorg. Chem.,*1994, **33**, 2456; (o) F. G. N. Cloke, C. I. Dalby, P. J. Daff and J. C. Green, *J. Chem. Soc. Dalton Trans.,*1991, 181; (p) F. G. N. Cloke, C. I. Dalby, M. J. Henderson, P. B. Hitchcock, C. H. L. Kennard, R. N. Lamb and C. L. Raston, *J. Chem. Soc. Chem. Commun.,* 1990, 1394 and references therein; (q) W. Kaim, S. Ernst and V. Kasack. *J. Am. Chem. Soc.,* 1990, **112**, 173; (r) W. Kaim, *Coord. Chem. Rev.,* 1987, **76**, 187; (s) C. Creutz, *Comments Inorg. Chem.,* 1982, **1**, 293.

5 (a) Y. Liu, P. Yang, J. Yu, X-J. Yang, J. D. Zhang, Z. Chen, H. F. Schaefer, B. Wu, *Organometallics*, 2008, **27**, 5830; (b) S. Greulich, A. F. Stange, H. Stoll, J. Fiedler, S. Záliš and W. Kaim, *Inorg. Chem.,* 1996, **35**, 3998.

6 (a) S. C. Patra, T. Weyhermüller and P. Ghosh, *Inorg. Chem.,* 2014, **53**, 2427; (b) A. S. Roy, H. M. Tuononen, S. P. Rath and P. Ghosh, *Inorg. Chem.,* 2007, **46**, 5942.

7 (a) T. Storr, E. C. Wasinger, R. C. Pratt and T. D. P. Stack, *Angew. Chem. Int. Ed.,* 2007, **46**, 5198; (b) Y. Shimazaki, T. Yajima, F. Tani, S. Karasawa, K. Fukui, Y. Naruta and O. Yamauchi, *J. Am. Chem. Soc.,* 2007, **129**, 2559; (c) Y. Shimazaki, F. Tani, K. Fukui, Y. Naruta and O. Yamauchi, *J. Am. Chem. Soc.,* 2007, **125**, 10512.

8 (a) G. M. Sheldrick, *SHELXS-97*; Universität Göttingen: Germany, 1997. (b) G. M. Sheldrick, *SHELXL-97*; Universität Göttingen: Germany, 1997. (c) G. M. Sheldrick, *SHELXL-2013-2*; Universität Göttingen: Germany, 2013.

9 M. J. Frisch, G. W. Trucks, H. B. Schlegel, G. E. Scuseria, M. A. Robb, J. R. Cheeseman, J. A. Montgomery Jr., T. Vreven, K. N. Kudin, J. C. Burant, J. M. Millam, S. S. Iyengar, J. Tomasi, V. Barone, B. Mennucci, M. Cossi, G. Scalmani, N. Rega, G. A. Petersson, H. Nakatsuji, M. Hada, M. Ehara, K. Toyota, R. Fukuda, J. Hasegawa, M. Ishida, T. Nakajima, Y. Honda, O. Kitao, H. Nakai, M. Klene, X. Li, J. E. Knox, H. P. Hratchian, J. B. Cross, V. Bakken, C. Adamo, J. Jaramillo, R. Gomperts, R. E. Stratmann, O. Yazyev, J. A. Austin, R. Cammi, C. Pomelli, J. W. Ochterski, P. Y. Ayala, K. Morokuma, G. A. Voth, P. Salvador, J. J. Dannenberg, V. G. Zakrzewski, S. Dapprich, A. D. Daniels, M. C. Strain, O. Farkas, D. K. Malick, A. D. Rabuck, K. Raghavachari, J. B. Foresman, J. V. Ortiz, Q. Cui, A. G. Baboul, S. Clifford, J. Cioslowski, B. B. Stefanov, G. Liu, A. Liashenko, P. Piskorz, I. Komaromi, R. L. Martin, D. J. Fox, T. Keith, M. A. Al-Laham, C. Y. Peng, A. Nanayakkara, M. Challacombe, P. M. W. Gill, B. Johnson, W. Chen, M. W. Wong, C. Gonzalez and J. A. Pople, *Gaussian 03*, revision E.01, Gaussian, Inc., Wallingford, CT, 2004.

10 (a) D. R. Salahub and M. C. Zerner, *The Challenge of d and f Electrons,* ACS, Washington, D.C., 1989; (b) R. G. Parr and W. Yang, *Density Functional Theory of Atoms and Molecules,* Oxford University Press, Oxford, UK, 1989; (c) W. Kohn and L. J. Sham, *Phys. Rev.,* 1965, **140**, A1133; (d) P. Hohenberg and W. Kohn, *Phys. Rev.,* 1964, **136**, B864.

11 (a) R. E. Stratmann, G. E. Scuseria and M. Frisch, *J. Chem. Phys.,* 1998, **109**, 8218; (b) M. E. Casida, C. Jamoroski, K. C. Casida and D. R. Salahub, *J. Chem. Phys.,* 1998, **108**, 4439; (c) R. Bauernschmitt and R. Ahlrichs, *Chem. Phys. Lett.,* 1996, **256**, 454.

12 (a) A. D. Becke, *J. Chem. Phys.,* 1993, **98**, 5648; (b) B. Miehlich, A. Savin, H. Stoll and H. Preuss, *Chem. Phys. Lett.,* 1989, **157**, 200; (c) C. Lee, W. Yang and R. G. Parr, *Phys. Rev. B,* 1988, **37**, 785.

13 P. Pulay, *J. Comput. Chem.,* 1982, **3**, 556.

14 H. B. Schlegel and J. J. McDouall, in *Computational Advances in Organic Chemistry,* ed. C. Ogretir and I. G. Csizmadia, Kluwer Academic, The Netherlands, 1991, 167.

15 (a) P. J. Hay and W. R. Wadt, *J. Chem. Phys.,* 1985, **82**, 270; (b) W. R. Wadt and P. J. Hay, *J. Chem. Phys.,* 1985, **82**, 284; (c) P. J. Hay and W. R. Wadt, *J. Chem. Phys.,* 1985, **82**, 299.

16 (a) V. A. Rassolov, M. A.Ratner, J. A. Pople, P. C. Redfern and L. A. Curtiss, *J. Comp. Chem.,* 2001, **22**, 976; (b) M. M. Francl, W. J. Pietro, W. J. Hehre, J. S. Binkley, D. J. DeFrees, J. A. Pople and M. S. Gordon, *J. Chem. Phys.,* 1982, **77**, 3654; (c) P. C. Hariharan and J. A. Pople, *Mol. Phys.,* 1974, **27**, 209; (d) P. C. Hariharan and J. A. Pople, *Theo. Chim. Acta.,*1973, **28**, 213; (e) W. J. Hehre, R. Ditchfield and J. A. Pople, *J. Chem. Phy.,* 1972, **56**, 2257.

17 (a) V. Rassolov, J. A. Pople, M. Ratner and T. L. Windus, *J. Chem. Phys.,* 1998, **109**, 1223; (b) M. M. Francl, W. J. Petro, W. J. Hehre, J. S. Binkley, M. S.Gordon, D. J. DeFrees and J. A. Pople, *J. Chem. Phys.,*1982, **77**, 3654; (c) P. C. Hariharan and J. A. Pople, *Theoret. Chimica Acta.*, 1973, **28**, 213.

18 N. M. O'Boyle, A. L. Tenderholt and K. M. Langner, *J. Comput. Chem.,* 2008, **29**, 839.

19 (a) M. Cossi, N. Rega, G. Scalmani and V. Barone, *J. Comput. Chem.,* 2003, **24**, 669; (b) V. Barone and M. Cossi, *J. Phys. Chem. A.,* 1998, **102**, 1995.

20 (a) T. A. Stephenson and G. Wilkinson, *J. Inorg. Nucl. Chem.,* 1966, **28**, 945; (b) P. R. Hoffman and K. G. Caulton, *J. Am. Chem. Soc.,* 1975, **97**, 4221.

21 S. C. Patra, M. K. Biswas, A. N. Maity and P.Ghosh, *Inorg. Chem.,* 2011, **50**, 1331.

22 (a) B. B. Wayland, A. E. Sherry and A. G. Bunn, *J. Am. Chem. Soc.,* 1993, **115**, 7675; (b) M. P. Garcia, M. V. Jimbnez, L. A. Ora, F. J. Lahoz, J. M. Casas and P. J. Alonso, *Organometallics,* 1993, **12**, 3257; (c) M. Gerisch, J. R. Krumper, R. G. Bergman and T. D. Tilley, *Organometallics,* 2003, **22**, 47; (d) S. Berger, A. Klein, M. Wanner and W. Kaim, *Inorg. Chem.,* 2000, **39**, 2516; (e) W. J. McCarty, X. Yang and R. A. Jones, *Chem. Commun.,* 2011, **47**, 12164; (f) M. Feller, E. Ben-Ari, T. Gupta, L. J. W. Shimon, G. Leitus, Y. Diskin-Posner, L. Weiner and D. Milstein, *Inorg. Chem.,* 2007, **46**, 10479; (g) M. Gerisch, J. R. Krumper, R. G. Bergman and T. D. Tilley, *J. Am. Chem. Soc.,* 2001, **123**, 5818; (h) J. P. Collman and R. Boulatov, *J. Am. Chem. Soc.,* 2000, **122**, 11812; (i) K. R. Dunbar and S. C. Haefner, *Organometallics,* 1992, **11**, 1431; (j) R. T. Hamazawa, T. Nishioka, I. Kinoshita, T. Takui, R. Santo and A. Ichimura, *Dalton Trans.*, 2006, 1374.

23 (a) A. Grupp, M. Bubrin, F. Ehret, Q. Zeng, F. Hartl, H. Kvapilová, S. Zális˘and W. Kaim, *Eur. J. Inorg. Chem.,* 2014, 110; (b) S. Patra, B. Sarkar, S. Ghumaan, M. P. Patil, S. M. Mobin, R. B. Sunoj, W. Kaim and G. K. Lahiri, *Dalton Trans.,* 2005, 1188; (c) S. Patra, B. Sarkar, S. M. Mobin, W. Kaim and G. K. Lahiri, *Inorg. Chem.*, 2003, **42**, 6469.

24 N. Muresan, K. Chlopek, T. Weyhermüller, F. Neese and K. Wieghardt, *Inorg. Chem.,* 2007, **46**, 5327.

25 Gas phase geometry of $L^{Ph}H_2$ was optimized with singlet spin state using 6-31G basis set to calculate the bond lengths of a neutral diimine ligand. The calculated –C=N- and =CH-CH= lengths are 1.280 and 1.474 Å. (For optimized geometry, optimized coordinate, see ref 6a)

26 P. Kubelka, F. Z. Munk, *Tech. Phys.,* 1931, **12**, 593.

Graphical contents entry

Molecular and electronic structures of the ruthenium, osmium and rhodium complexes of 1,4-di(3-nitrophenyl)-1,4-diazabutadiene (LDAB) and their redox series are reported.